A Harmonic Gradient Method for Unsteady Supersonic Flow Calculations

Ping-Chih Chen*
Northrop Corporation, Hawthorne, California
and
D. D. Liu†
Arizona State University, Tempe, Arizona

An accurate and effective method for calculations of unsteady three-dimensional supersonic flow has been developed. The present method is capable of handling general cases of planar, coplanar, and nonplanar wing planforms in the complete frequency domain. A harmonic-gradient potential model is provided for elementary doublet panels to be made compatible with the wave number generated. Consequently the number of panel elements required is least affected by the given Mach number and reduced frequency. Thus, the required panel number can be optimized to as few as 30, a fraction of the number required by the existing methods. To assess the accuracy and effectiveness of the present method, comparison with various available data is given.

Nomenclature

ΔC_P	= lifting pressure coefficient
h	= structural mode shapes
i	$= \sqrt{-1}$
L	= reference chord length
m	= slope of leading or trailing edge of the panel element
M	= freestream Mach number
(x,y,z)	= wing-fixed coordinates; $(x,y,z) = (X/\beta L,\ Y/L,\ Z/L)$ (see Fig. 1)
(x_0,y_0,z_0)	= control point location in (x,y,z) coordinates
(X,Y,Z)	= true physical coordinates
α	= position of leading or trailing edge of the panel element at $\eta = 0$
β	$= \sqrt{M^2 - 1}$
(ξ,η,ζ)	= moving coordinates (see Fig. 1)
ψ	= oscillatory potential
Φ	= modified velocity potential $= \psi e^{ikMX}$
$\Delta\Phi$	= doublet solution of modified potential
ω	= circular frequency of harmonic motion

Subscripts

i	= index of the number of chordwise element in the jth strip
j	= index of the number of strip
T.E.	= trailing edge of the wing
w	= wake

I. Introduction

AFTER 35 years of supersonic flight, a need still exists for a reliable prediction of unsteady airload on interfering lifting surface configurations in supersonic flow. Although requirements for subsonic flutter analysis of interfering configurations are satisfied by the doublet-lattice method,[1] an equally effective supersonic method has been lacking.

Supersonic numerical lifting surface methods can be divided into three categories: those that adopt 1) the velocity potential, 2) the acceleration potential, and 3) the gradient of the velocity potential as the dependent variable. Typical of the first method is the Mach-box method, whose shortcomings include the fact that the velocity potential must be determined off of the planform in the so-called diaphragm regions. The supersonic doublet-lattice method of Giesing and Kalman[2] and the kernel-function method of Cunningham[3,4] belongs to the second category. In Ref. 2, questions are still unanswered about the selection of downwash control point locations as well as correlations with two-dimensional solutions. In Ref. 3, the method has been widely accepted except that its results are sensitive to the choice of pressure modes which are more varied in number and form at supersonic speeds rather than at subsonic.

In the third category, the potential-gradient method (PGM) of Jones and Appa[5] has shown promise of this approach to interfering nonplanar configurations. The PGM permits an exact idealization of the planform(s), without any need for assumption of pressure modes, and can utilize the automatic grid-generation scheme that has been developed for the subsonic doublet-lattice method. However, Ref. 5 is limited by a series expansion scheme in the supersonic kernel and hence ceases to be valid in the higher-frequency domain as well as for the low supersonic Mach numbers. Recent work of Hounjet[6] extended the PGM to higher-frequency domain by using the Laschka's exponential series representation in the supersonic kernel of Harder and Rodden.[8,13] Although Hounjet has improved the validity of PGM in almost all his calculation cases, no fewer panel elements are required for convergence than those used by Jones and Appa.

On the other hand, the present development of the harmonic-gradient (H-G) method is motivated by the aeroelastic requirements set by the configurations of modern fighter-aircraft and those of the new generation missile/fin combination. In the former case, the complex canard wing multiple-tails interaction warrants accurate prediction of supersonic flutter boundaries. In the latter cases, the fin-body or wing-body configuration could be susceptible to aeroelastic instability as a result of combined body bending-fin torsion motion during the supersonic cruising phase. Consequently a

Presented as Paper 83-0887 at the AIAA/ASME/ASCE/AHS 24th Structures, Structural Dynamics & Materials Conference, Lake Tahoe, Nev., May 2-4, 1983; received July 24, 1984; revision received Jan. 2, 1985.

*Senior Engineer, Aircraft Division. Formerly Graduate Student, Arizona State University. Member AIAA.

†Associate Professor, Department of Mechanical and Aerospace Engineering. Member AIAA.

considerable amount of panels will be required for modeling a complete configuration in order to perform a full-scale aeroelastic analysis. Such modeling mandates a cost effective panel method particularly for unsteady aerodynamic predictions. Because of the consistent formulation of the harmonic gradient model, the present method is least affected by the given Mach number and the range of reduced frequency compared to other methods. As will be seen in the later analysis of this paper, the present H-G method not only reduces the panel number substantially but yields improved accuracy in almost all cases.

II. Formulation

The Supersonic Integral

Following the basic formulation of Jones,[7] there is obtained the integral solution of the oscillatory supersonic linearized equation in the frequency domain:

$$\psi(x_0,y_0,z_0) = -\frac{1}{2\pi}\frac{\partial}{\partial n}\iint_A \Delta\phi(x,y,z)H(\xi,\eta,\zeta)\mathrm{d}x\mathrm{d}y \tag{1}$$

where ψ is the oscillatory potential and $\Delta\phi$ is the doublet solution to be sought. The supersonic kernel function H is obtained from the elementary solution, i.e.,

$$H(\xi,\eta,\zeta) = \frac{\cos kR}{R}\, e^{-ikM\xi} \tag{2}$$

where $k = \mathrm{MK}/\beta$ and K is the reduced frequency, $K = \omega L/U_\infty$; and R is defined as

$$R = [\xi^2 - \eta^2 - \zeta^2]^{1/2} \tag{3}$$

and

$$\xi = x_0 - x, \quad \eta = y_0 - y, \quad \zeta = z_0 - z \tag{4}$$

The operator $\dfrac{\partial}{\partial n}$ can be expressed as

$$\frac{\partial}{\partial n} = -\ell_y\frac{\partial}{\partial y_0} - \ell_z\frac{\partial}{\partial z_0} = -\ell_y\frac{\partial}{\partial \eta} - \ell_z\frac{\partial}{\partial \zeta} \tag{5}$$

where ℓ_y and ℓ_z are the direction cosines of the normal at any point on the planforms. Notice that in Eq. (1), (x_0,y_0,z_0) and (x,y,z) represent the field point and the source sending point, respectively. Also, Eq. (1) is to integrate over the area A, which encloses all sending points that originate from both the wing panels and wakes within the inverse Mach cone of influence (Fig. 1).

Next, for convenience we define a kernel integral function S, i.e.,

$$S(\xi,r) = -\int_\xi^r \frac{\cos(k\sqrt{\tau^2 - r^2})}{\sqrt{\tau^2 - r^2}}\mathrm{d}\tau \tag{6}$$

where $r = (\eta^2 + \zeta^2)^{1/2}$.

According to the area A defined by the inversed Mach cone, the inner integral of Eq. (1) has the integration limit from the given leading edge $x = L(y)$ to $R = 0$. The boundary conditions require $\Delta\phi = 0$ at $x = L(y)$ and $S(r,r) = 0$ at the Mach cone. With these conditions, we then integrate Eq. (1) by parts and obtain

$$\psi(x_0,y_0,z_0) = \frac{1}{2\pi}\frac{\partial}{\partial n}\iint_{x=L(y)}^{x=x_0\pm r}\frac{\partial}{\partial x}[\Delta\phi\cdot e^{-ikM\xi}]S(\xi,r)\mathrm{d}x\mathrm{d}y \tag{7}$$

The above equation is to be solved based on a finite-element approach similar to those in Refs. 5 and 6. For simplification of the computational procedure, the coordinate system (x,y,z) can be transformed into a moving one (ξ,η,ζ) whose origin is placed at a local center (x_0,y_0,z_0) on each panel being computed. Accordingly, Eq. (7) is recast as

$$\psi(x_0,y_0,z_0) = -\frac{1}{2\pi}\sum_{j=1}^{Q}\sum_{i=1}^{P}\frac{\partial}{\partial n}\int_{\eta_{j-1}}^{\eta_j} \times\int_{\xi_{i-1}}^{\xi_i}\frac{\partial}{\partial\xi}[\Delta\phi_{ij}e^{-ikM\xi}]S(\xi,r)\mathrm{d}\xi\mathrm{d}\eta \tag{8}$$

where Q indicates number of strips in the spanwise direction and P is the number of chordwise elements in the jth strip. The sending panel element is defined by $(\xi_{i-1}, \eta_{i-1}) < (\xi, \eta) < (\xi_i, \eta_i)$. The doublet solution $\Delta\phi_{ij}$ is to be modeled by the proposed harmonic-gradient formulation in the following section.

Harmonic-Gradient (H-G) Model

To evaluate Eq. (8), based on the given flow and downward conditions, requires careful treatment of the integrand. In particular, the basic modeling technique for the approximation of the first part of the integrand is the concern here.

In order to achieve computation accuracy and effectiveness for the oscillatory motion in the high-frequency range, it is important to render the doublet solution and its convective gradient uniformly valid throughout the complete frequency domain. This is to say that the doublet solution must be spatially harmonic. In so doing, the element size is made automatically compatible with the wave number generated along the chord; hence, we expect the doublet solution obtained can be least affected by the selected panel length. With this physical consideration, the doublet solution of the integrand in Eq. (8) can be modeled as

$$\frac{\partial}{\partial\xi}[\Delta\phi_{ij}] = b_{ij}e^{-ikMx} \tag{9}$$

Indeed, this harmonic-gradient model can be consistently expressed in terms of the moving coordinates, i.e.,

$$\frac{\partial}{\partial\xi}[\Delta\phi_{ij}e^{-ikM\xi}] = a_{ij}e^{-ikM\xi} \tag{10}$$

where a_{ij} and b_{ij} are complex constants representing the doublet strength to be determined for each panel element.

It should be remarked that in the PGM formulation of Refs. 5 and 6, both assumed that the convective gradient of the modified potential is constant, i.e.,

$$\frac{\partial}{\partial x}[\Delta\phi_{ij}e^{-ikMx}] = c_{ij} \tag{11}$$

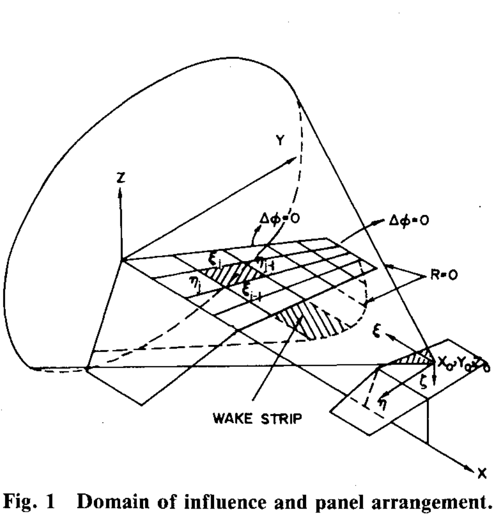

Fig. 1 Domain of influence and panel arrangement.

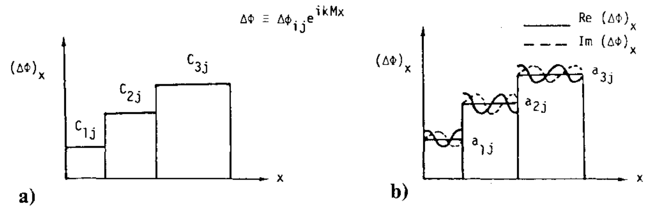

Fig. 2 Modeling of potential along chord: a) potential-gradient method, b) harmonic-gradient method.

As shown in Fig. 2, it can be seen that the above PGM assumption is no more than a special case of H-G model; Eq. (11) basically assumes the asymptotic form of Eq. (10), which is spatially nonoscillatory. Unless the selected panel size is made compatible with the given wave number, one should not expect accurate results in the high-frequency range. This then implies that the higher the given K, the smaller the panel size must be accommodated in order to achieve the computational accuracy. By contrast, the present H-G model removes this stringent requirement for panel size. Hence, it is demonstrated in our computations (Tables 1-4) that the same numerical accuracy can be achieved with many less panels assigned than with those of all the previous methods.

Moreover, unlike the present H-G formulation, the PGM condition, Eq. (11), is not fully expressed in the moving coordinates. As a result, Refs. 5 and 6 would suffer from other computational shortcomings. This will be discussed further in the next section.

Downwash

H-G model Eq. (10) is applied to Eq. (8), the downwash velocity can be expressed as

$$\bar{w}=\frac{\partial\psi}{\partial z_0}=[\ell_y V(x_0,y_0,z_0)+\ell_z W(x_0,y_0,z_0)] \tag{12}$$

where

$$w(x_0,y_0,z_0)=-\frac{1}{2\pi}\sum_{i,j}\int_{\eta_{j-1}}^{\eta_j}\int_{\xi_{i-1}}^{\xi_i} \times e^{-ikM\xi}[\Omega_0\cdot S+\zeta^2\Omega_1\cdot S]\,a_{ij}\,\mathrm{d}\xi\mathrm{d}\eta \tag{13}$$

and

$$V(x_0,y_0,z_0)=-\frac{1}{2\pi}\sum_{i,j}\zeta\int_{\xi_{i-1}}^{\xi_i} e^{-ikM\xi}[\Omega_0\cdot s]\int_{\eta_{j-1}}^{\eta_j}\mathrm{d}\xi \tag{14}$$

The symbols Ω_0 and Ω_1 are the planar and the nonplanar operators, respectively, defined as

$$\Omega_0=\frac{1}{r}\frac{\partial}{\partial r}$$

$$\Omega_1=\frac{1}{r}\frac{\partial}{\partial r}\left(\frac{1}{r}\frac{\partial}{\partial r}\right)$$

Now, some words are in order to distinguish the basic difference in the downwash formulation between the H-G model and that of PGM. For a given mode shape $h(x,y,z)$, a descriptive expression of Eq. (12) should read:

$$\left(-\frac{\partial}{\partial\xi}+iK\right)h=\frac{\partial}{\partial z_0}=\frac{1}{2\pi}\frac{\partial^2}{\partial n\partial\zeta}\iint\frac{\partial}{\partial\xi} \times[\Delta\phi e^{-ikM\xi}]S(\xi,r)\mathrm{d}\xi\mathrm{d}\eta \tag{15}$$

in which the left-hand side is evaluated at the control point $(\xi,\eta,\zeta)=(0,0,0)$ for each panel. Recall the downwash equation expressed in PGM

$$\left(\frac{\partial}{\partial x}+ik\right)h\cdot e^{ikMx_0}=\frac{\partial\Phi}{\partial z_0}$$

$$=-\frac{1}{2\pi}\frac{\partial^2}{\partial n\partial z_0}\iint\frac{\partial}{\partial x}(\Delta\Phi)S(\xi,r)\mathrm{d}\xi\mathrm{d}\eta \tag{16}$$

where Φ is the so-called modified potential. Although the PGM has made use of the moving coordinate for convenience of computation, clearly Eq. (16) is not formally derived in this system. More important, we found that the extra term, e^{ikMx_0} on the LHS, which perhaps resulted from an inconsistent treatment of the coordinate system, indeed has created much trouble for solution convergence in a number of cases. In fact, an inconsistent formulation of the problem would yield an explicit x_0-dependent equation such as Eq. (16), whereas a consistent formulation in the moving coordinates leads it naturally to the construction of the H-G model. As in the H-G formulation of Eq. (15), it avoids the explicit dependence on the (x,y,z) coordinates altogether.

III. Analysis

Planar Case ($\zeta=0$)

The crux of the planar integral lies in the evaluation of the integrand $\Omega_0 S$. The fact that the kernel integral S involving an integral limit at Mach cone surface requires some cases in differentiation which amounts to Hadamards' method of finite part integral. Applying Hadamards' procedure to the operator $\Omega_0 S$ and after some manipulation, we arrive at two basically regular terms,

$$\Omega_0 S=-(1/r^2)[L_0+L_1] \tag{17}$$

where

$$L_0=[\xi\cos(k\sqrt{\xi^2-r^2})]/\sqrt{\xi^2-r^2} \tag{18}$$

$$L_1=\int_r^{\xi}k\sin[k\sqrt{\tau^2-r^2}]\,\mathrm{d}\tau \tag{19}$$

Now, applying the transformation

$$u=[\sqrt{\tau^2-r^2}]/r$$

to Eq. 19 yields

$$L_1=kr\int_0^{(\sqrt{\xi^2-r^2})/r}[u/\sqrt{u^2+1}]\sin[(kr)u]\,\mathrm{d}u \tag{20}$$

As suggested by Harder and Rodden,[8] Laschka's exponential series substitution can be used to integrate L_1, *i.e.*,

$$u/\sqrt{u^2+1}\simeq 1-\sum_{n=1}^{N}a_n\exp(-ncu) \tag{21}$$

where the constant c and the coefficients a_n have been redefined by Jordan[22] and recently by Desmarais[9] for cases up to $N=8$, 12, and 24 terms. With the Laschka-Desmarais series, L_1 can then be integrated throughout the Mach cone domain of influence.

Another type of singularity occurs at the Mach cone and the panel intersection. Specifically this happens when one performs chordwise integration in Eqs. (13) and (14) across each element in ξ. For example, the integration of L_0 reads

$$L_2(\eta)=\int_{\xi(\eta)_{i-1}}^{\xi(\eta)_i}e^{-ikM\xi}(L_0+L_1)\mathrm{d}\xi \tag{22}$$

which has a singular line at $\xi = r$ as the Mach cone intersects the ith panel between ξ_{i-1} and ξ_i. This type of singularity is an integrable one; hence, integration by parts of the above yields two regular terms, i.e.,

$$L_2(\eta) = \sin k\sqrt{\xi^2 - r^2}\cdot [ke^{ikM\xi}]^{-1}\Big|_{\xi(\eta)_{i-1}}^{\xi(\eta)_i} + \int_{\xi(\mu)_{i-1}}^{\xi(\mu)_i} [iM\sin(k\sqrt{\xi^2 - r^2}) + L_1] e^{-ikM\xi}\mathrm{d}\xi \qquad (23)$$

Clearly L_2 represents the chordwise integration. Since L_2 is now regular, it can be integrated numerically by means of, say, Gaussian quadrature. It should be cautioned that its lower integration limit is to be replaced by $\xi = r$ whenever the limit exceeds the Mach cone. The value of $\xi_i(\eta)$ and $\xi_{i-1}(\eta)$ are determined by $m_i\eta + \alpha_i$ and $m_{i-1}\eta + \alpha_{i-1}$, which define the leading edge and trailing edge of the ith element, respectively.

Lastly, the spanwise integration of Eq. (13) is complicated by a dipole-like singularity at $r = 0$. This type of singularity exists only in the planar case and is common to both supersonic panels and subsonic panels. Except in the former case, all singularities occur in the element considered together with all preceding elements along the chordwise strip within the influence domain. Hence, following Rodden et al.,[1] we use a parabolic fit of $L_2(\eta)$ to evaluate this singular integral across a narrow strip in the singular region of the element, i.e.,

$$\int_{-\epsilon}^{\epsilon} \frac{1}{r^2} L_2(\eta)\mathrm{d}\eta \simeq \int_{-\epsilon}^{\epsilon} \frac{1}{r^2}(A\eta^2 + B\eta + C)\mathrm{d}\eta \qquad (24)$$

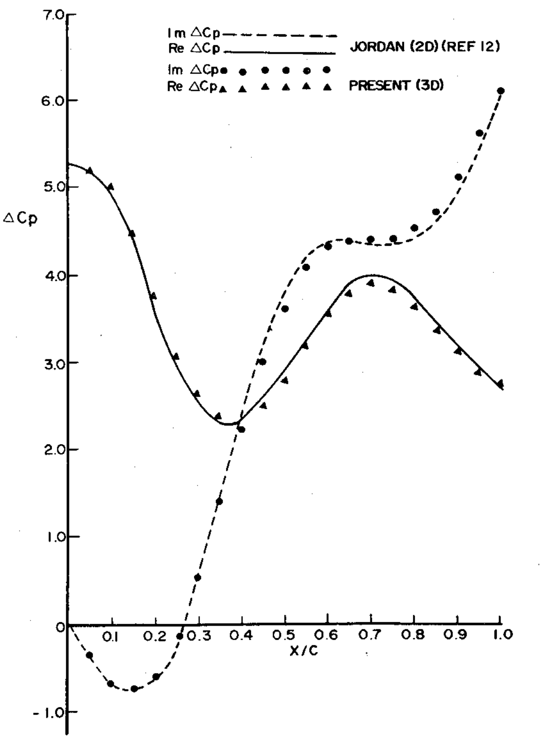

Fig. 3 Comparison of unsteady pressure with Jordan's two-dimensional method at $M = 1.25$ and $K = 2.0$; pitching axis at the leading edge.

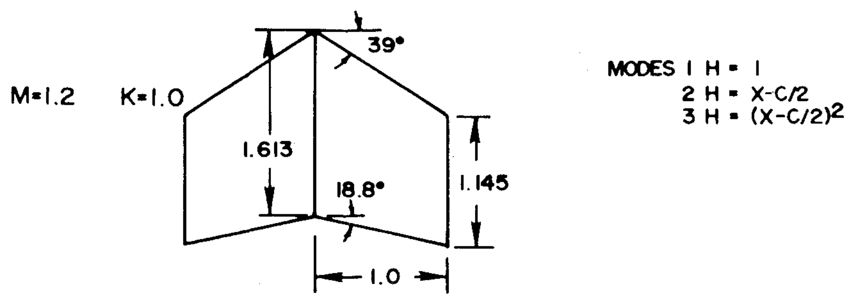

Table 1 AGARD swept wing at $M = 1.2$ and $K = 1.0$ with three modes

Methods Elements		Present (150)	Present (100)	Present (50)	Present (30)	Ref. 6 (150)	Ref. 5 (147)	Ref. 14 (600)	Ref. 15 (1734)
Q_{11}	MOD	3.705	3.689	3.807	3.775	3.697	3.486	3.570	3.665
	ARG*	95.68	95.54	94.42	94.21	98.34	100.16	96.50	95.78
Q_{21}	MOD	0.93	0.9343	0.982	0.9715	0.891	1.012	0.868	0.904
	ARG	143.1	142.1	139.9	138.0	143.43	147.82	144.70	143.00
Q_{31}	MOD	0.91	0.909	0.935	0.9341	0.916	0.946	0.877	0.912
	ARG	111.1	111.5	110.1	110.3	114.28	113.95	112.79	112.57
Q_{12}	MOD	4.502	4.479	4.613	4.604	4.575	4.492	4.370	4.490
	ARG	21.21	21.39	20.54	20.64	24.04	24.98	21.24	21.02
Q_{22}	MOD	2.008	2.001	2.074	2.048	1.966	2.040	1.914	1.983
	ARG	64.59	64.09	62.73	60.77	65.78	64.06	65.75	64.37
Q_{32}	MOD	1.298	1.306	1.344	1.382	1.335	1.291	1.255	1.313
	ARG	43.55	43.95	43.22	41.97	45.36	41.53	43.47	43.52
Q_{13}	MOD	2.78	2.824	2.949	3.031	2.892	2.644	2.572	2.720
	ARG	5.699	6.168	5.750	4.262	4.75	−0.30	3.48	3.69
Q_{23}	MOD	2.298	2.291	2.365	2.354	2.333	2.008	2.213	2.301
	ARG	3.812	4.23	4.051	1.736	5.39	2.36	2.58	2.94
Q_{33}	MOD	1.378	1.393	1.455	1.462	1.378	1.218	1.270	1.346
	ARG	21.09	20.66	20.10	14.27	20.03	24.88	20.09	19.85

*Degrees

It turns out that this technique works out equally well for the supersonic case.

Nonplanar Case ($\zeta \neq 0$)

The nonplanar integral in Eq. (13) reads

$$\Omega_I S = \frac{I}{r}\frac{\partial}{\partial r}(\Omega_0 \cdot S) = \Omega_0 \cdot \left(-\frac{I}{r^2}\right)(L_0 + L_I) \tag{25}$$

Clearly $\Omega_I S$ involves higher-order differentiation than $\Omega_0 S$ does. However, to derive the complete expression of the nonplanar integral only requires laborious algebriac manipulations. Since the singularities involved are all integrable ones, one can evaluate Eq. (25) following essentially the similar procedure to that of the planar case.

Wake Treatment

As the wake sustains no lift, this implies that $\Delta C_p = 0$ across the wake. Thus, the doublet solution on wake can be expressed as

$$\Delta\phi_w = \Delta\phi_{\text{T.E.}} \exp[ik\beta^2 \xi_{\text{T.E.}}/M] \tag{26}$$

where $\Delta\phi_w$ and $\Delta\phi_{\text{T.E.}}$ represent $\Delta\phi$ on the wake and at the trailing edge, respectively.

The doublet strength $\Delta\phi_{\text{T.E.}}$ of a given jth strip, according to the H-G model, can be expressed in terms of a_{ij}, i.e.,

$$(\Delta\phi_{\text{T.E.}})_j = a_{pj} - \sum_{i=1}^{p} [a_{ij} - a_{(i-1)j}] \cdot e^{-ikM(\xi_{i-1} - \xi_i)}/ikM \tag{27}$$

For each given jth strip, Eq. (27) can be expressed in terms of a matrix equation

$$\{(\Delta\phi_{\text{T.E.}})_j\} = [E_{j,ij}]\{a_{ij}\} \tag{28}$$

where in the case of $i = P$, Eq. (28) reduces to Eq. (27). Combining Eqs. (26) and (7) and following the similar evaluation procedures for $\bar{W}$ yield the downwash contribution $\bar{W}_w$ from the wake.

Kinematic Boundary Conditions

For a given mode shape h the unknown doublet strength a_{ij} in Eq. (10) can be evaluate by the following matrix equation, i.e.,

$$[[\bar{W}] + [\bar{W}_w][E_{j,ij}]]\{a_{ij}\} = \{(h_x + iKh)_{ij}\} \tag{29}$$

and the b_{ij} in Eq. (9) can be obtained in terms of a_{ij} by the following recurrence formula

$$b_{nj} = -\sum_{\nu=1}^{n} (a_{\nu j} - a_{(\nu-1)j})/\exp[ikM \sum_{i-1}^{\nu} (x_i - x_{i-1})] \tag{30}$$

Pressure and Generalized Forces

The pressure coefficient ΔC_p can be related to the doublet strength a_{ij} and b_{ij} defined in Eqs. (9) and (10), i.e.,

$$\Delta C_{p_{ij}}[x_i] = (\beta/M^2)a_{ij} - (ik/M\beta)b_{ij}e^{-ikMx_i} \tag{31}$$

and the generalized forces are given by

$$Q_{IJ} = \sum_{ij} \Delta y_j \int_{x_{i-1}}^{x_i} h^{(I)}(x)\Delta C_{p_{ij}}^{(J)}(x)\mathrm{d}x \tag{32}$$

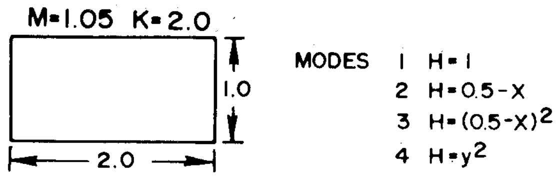

Table 2 Rectangular wing at $M = 1.05$ and $K = 2.0$ with four modes

Methods Elements		Present (200)	Present (100)	Present (50)	Ref. 16 (311)	Ref. 14 (544)
Q_{11}	MOD	6.328	6.462	6.484	6.238	5.992
	ARG	97.28	95.79	101.3	94.3	94.2
Q_{21}	MOD	3.851	3.932	3.935	3.851	3.68
	ARG	−167.6	−168.7	−161.3	−173.3	173.3
Q_{31}	MOD	0.480	0.499	0.658	0.289	0.285
	ARG	2.80	2.926	12.05	13.3	13.0
Q_{41}	MOD	1.716	1.828	1.813	1.73	1.546
	ARG	106.5	105.2	109.2	103.7	104.0
Q_{12}	MOD	0.698	0.709	0.670	0.749	0.703
	ARG	23.89	23.67	32.4	17.08	16.6
Q_{22}	MOD	0.913	0.930	0.878	0.96	0.904
	ARG	86.26	85.49	91.7	80.59	80.7
Q_{32}	MOD	0.626	0.642	0.623	0.646	0.61
	ARG	167.3	166.4	174.3	157.8	158.8
Q_{42}	MOD	0.233	0.247	0.226	0.251	0.2256
	ARG	37.75	36.32	43.36	30.02	31.53
Q_{13}	MOD	0.639	0.656	0.661	0.619	0.587
	ARG	88.67	87.4	95.8	83.8	83.4
Q_{23}	MOD	0.3179	0.326	0.344	0.303	0.283
	ARG	174.7	173.5	−177.1	168.2	168.0
Q_{33}	MOD	0.1139	0.116	0.095	0.116	0.1149
	ARG	84.37	83.12	85.1	82.6	81.2
Q_{43}	MOD	0.176	0.187	0.187	0.174	0.153
	ARG	94.2	93.26	100.9	89.67	88.9
Q_{14}	MOD	1.716	1.828	1.813	1.735	1.55
	ARG	106.5	105.2	109.2	103.7	103.7
Q_{24}	MOD	1.084	1.154	1.134	1.112	0.99
	ARG	−157.0	−158.3	−152.4	−162.7	−162.2
Q_{34}	MOD	0.179	0.188	0.224	0.132	0.127
	ARG	2.308	0.9758	12.54	160.0	162.6
Q_{44}	MOD	0.846	0.931	0.89	0.896	0.743
	ARG	126.0	124.3	127.0	122.2	123.4

where $h^{(I)}(x_i)$ is the Ith structural mode, $\Delta C_{p_{ij}}^{(J)}(x_i)$ is the pressure due to the Jth mode, and Δy_j is the span width of the panel element considered.

IV. Results and Discussion

To assess the accuracy of the H-G solution and to demonstrate the computational efficiency and effectiveness of the present method, various examples of a wide class of wing planforms are given in Figs. 3-7, together with Tables 1-4. Correlations with other available data are also presented. Without loss of generality, the reference chord length L in all the following numerical cases is set to unity for convenience.

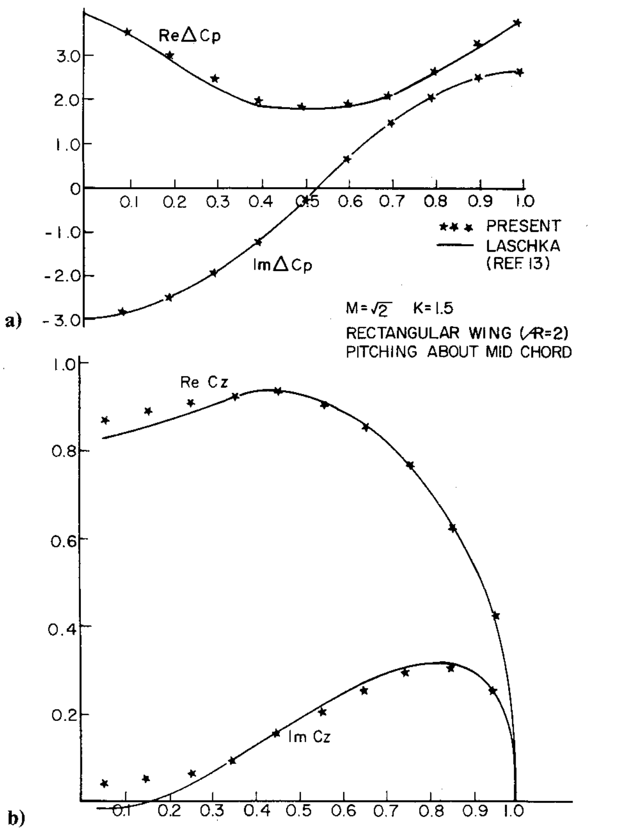

Fig. 4 Unsteady pressure distribution of an aspect-ratio-two rectangular wing at $M=2.0$ and $K=1.5$; pitching axis at the midchord: a) pressure distribution along midsection; b) spanwise distributions of unsteady normal load.

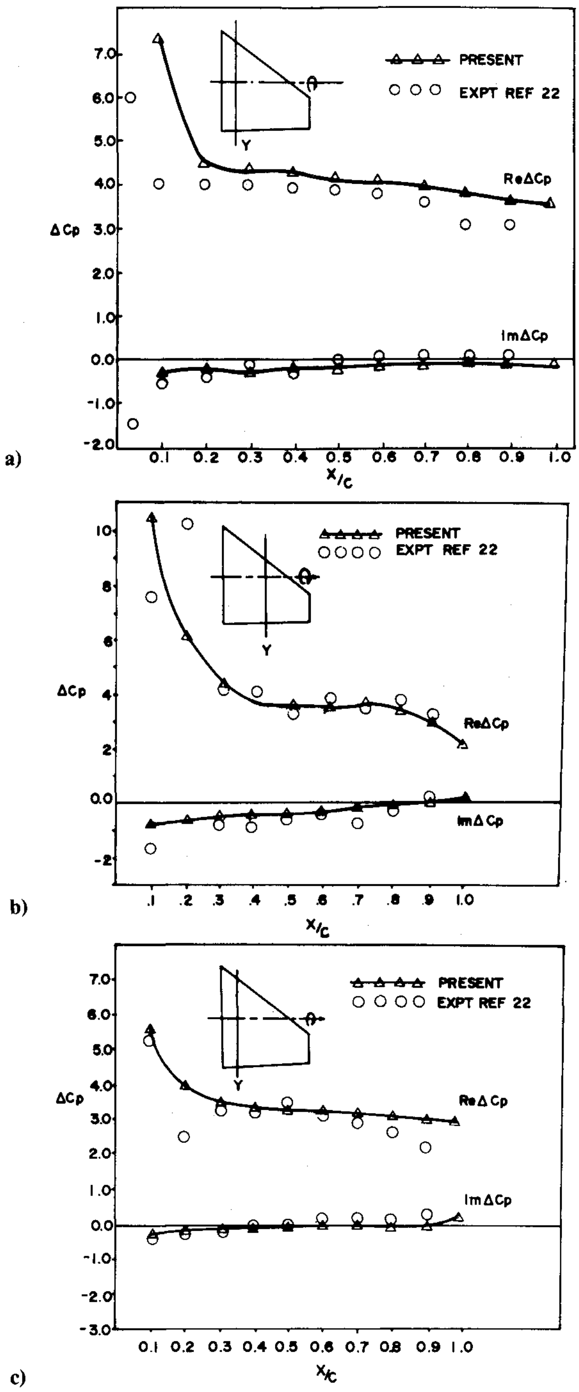

Fig. 5 Comparison of computed unsteady pressure on a Northrop F-5 wing with measured data of NLR: a) $M=1.328$, $K=0.1$, and $Y=18.1\%$; b) $M=1.188$, $K=0.11$, and $Y=18.1\%$; c) $M=1.188$, $K=0.11$, and $Y=50\%$.

Verification of Accuracy

To verify the present results with other existing methods, two typical cases are selected for comparison. First, we have compared the present results with the exact linearized solutions in Ref. 20 and those of Miles in Ref. 21 for delta wings with subsonic, sonic, and supersonic leading edges in steady lifting flow as well as in slowly oscillatory flow, respectively. We found that all results for pressures, forces, and damping-in-pitch moments check well with the above theoretical results. Second, the computed in-phase and the out-of-phase pressures at the root-chord section of a high-aspect-ratio rectangular wing have been compared with various available two-dimensional results. These include: Chadwick-Platzer[11] and Liu and Pi[10] for cases of $M=1.15$, $K=0.4$, 1.2, and $M=1.5$, $K=0.832$, 1.25, with pitching axis at leading edge and at mid-chord, respectively, and Jordon[12] for cases of $M=1.25$, $K=2.0$ in plunging mode and in pitching mode. Again we have found that the present H-G results are in excellent agreement with all the above cases. One such typical comparison is presented in Fig. 3. Figure 4a shows the root-chord pressure of an aspect-ratio-two rectangular wing; Fig. 4b shows the spanwise normal force distribution. Also, good agreement is observed between the present results and those of Laschka.[13]

Computational Efficiency and Effectiveness

In contrast to the previous methods, the present method, because of its H-G model, improves the computational efficiency by substantially reducing the number of panel elements used. Meanwhile, the same accuracy can be achieved in most cases.

Tables 1-4 summarize the generalized forces computed for the AGARD swept wing, rectangular wing, and wing-tail-fin combination. In Table 1, we use 150 panel elements to as few as 30 elements to compute the generalized forces $Q_{IJ}s$, whereas four previous methods[5,6,14,15] adopted 150 panel elements to as many as some 1700 elements. The present results using 30 elements agree well with all other methods. Table 2 presents the generalized forces for the rectangular wing oscillating in four selected modes at $M=1.05$ and $K=2.0$. Again, with 50 to 200 panel arrangements we have demonstrated that the present method at this low Mach number and moderately high frequency results in satisfactory comparison with those of Refs. 14 and 16.

In Table 3, three structural modes are used for the AGARD T-tail interferences, i.e., tail: $h_1=0$, $h_2=0$ and $h_3=Y$; fin: $h_1=Z^2$, $h_2=Z(X-0.875Z-3.0)$ and $h_3=0$.

In comparison with other data quoted, it is interesting to observe that all methods disagree in forces Q_{32} and Q_{31}. We

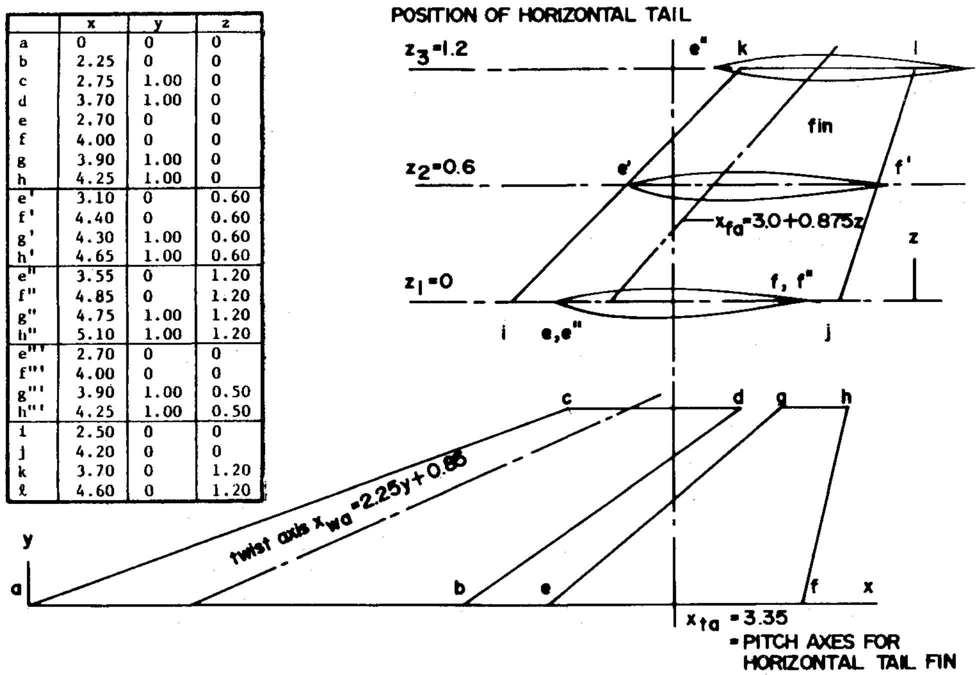

	x	y	z
a	0	0	0
b	2.25	0	0
c	2.75	1.00	0
d	3.70	1.00	0
e	2.70	0	0
f	4.00	0	0
g	3.90	1.00	0
h	4.25	1.00	0
e'	3.10	0	0.60
f'	4.40	0	0.60
g'	4.30	1.00	0.60
h'	4.65	1.00	0.60
e"	3.55	0	1.20
f"	4.85	0	1.20
g"	4.75	1.00	1.20
h"	5.10	1.00	1.20
e"'	2.70	0	0
f"'	4.00	0	0
g"'	3.90	1.00	0.50
h"'	4.25	1.00	0.50
i	2.50	0	0
j	4.20	0	0
k	3.70	0	1.20
ℓ	4.60	0	1.20

Fig. 6 AGARD wing-tail-fin combination.

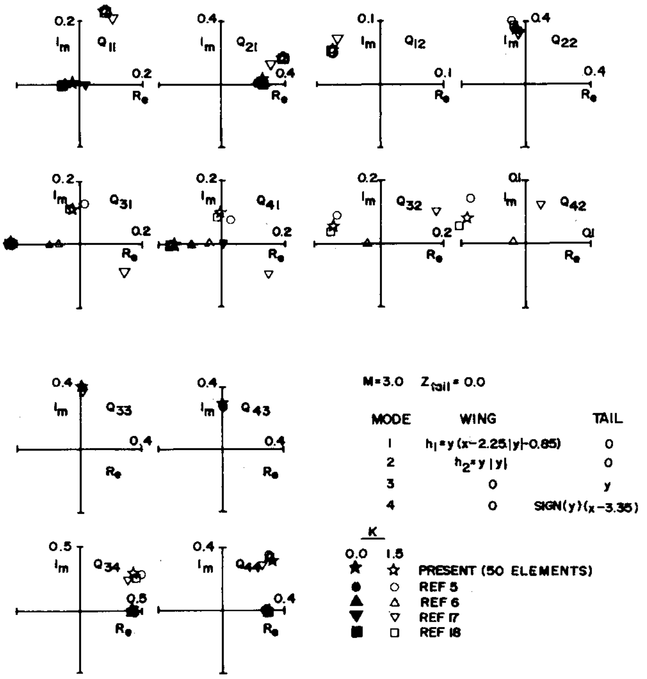

Fig. 7 Phase plane diagram for generalized aerodynamic coefficients (AGARD wing-tail configuration).

Table 3 AGARD fin-tail interference $Z_{\mathrm{TAIL}}=1.2$ at $M=1.6$ and $K=1.5$

Methods Elements		Present (100)	Present (50)	Ref. 6 (105)	Ref. 5 (105)	Ref. 19
Q_{11}	MOD	0.8203	0.8323	0.8238	0.7801	7.1943
	ARG	88.35	89.82	83.58	90.92	79.27
Q_{21}	MOD	0.1064	0.1117	0.0887	0.0905	0.2094
	ARG	119.0	116.6	128.55	131.93	71.51
Q_{31}	MOD	0.2056	0.2131	0.1026	0.1898	2.5818
	ARG	20.09	25.76	−62.56	72.84	79.67
Q_{12}	MOD	0.7133	0.7433	0.7115	0.6860	1.5532
	ARG	15.8	20.68	13.23	18.22	−24.23
Q_{22}	MOD	0.2597	0.2609	0.2600	0.2671	0.3924
	ARG	61.23	62.53	63.56	67.30	43.99
Q_{32}	MOD	0.1611	0.1775	0.0470	0.1397	0.3766
	ARG	−62.46	−51.27	−166.97	177.11	−68.31
Q_{13}	MOD	0.0848	0.0887	0.0954	0.0873	2.4391
	ARG	37.14	40.7	61.86	64.92	87.06
Q_{23}	MOD	0.0298	0.0305	0.0316	0.1812	0.0238
	MOD	21.87	24.45	48.18	7.90	27.75
Q_{33}	ARG	0.6493	0.6532	0.7177	0.6686	1.0056
	ARG	84.50	85.58	88.47	89.79	88.01

believe that the disagreement between the present results and those of Refs. 5 and 6 is probably caused by the explicit dependence on the exponential term e^{ikMx_0} in Eq. (16), which could be the source of numerical errors in Refs. 5 and 6.

Next, results for an AGARD wing-tail nonplanar case ($Z=0.6$) and coplanar case ($Z=0$) are presented in Table 4 and Fig. 7, respectively, The present results compare well with those of Ref. 18 in both cases. In Table 4, notice that there is little difference between results computed using 50 elements and 100 elements; again, this assures the cost-effectiveness of the H-G method in that the number of elements can be optimized and does not depend on Mach number and reduced frequency K. Lastly, it should be pointed out that Hounjet's result[6] correlates poorly with the present result for cases of $K=1.5$, whereas it correlates well for the case of $K=0$. The latter is expected as the e^{ikMx_0} term would vanish and contribute no error.

Correlation with Experimental Data

Finally, we compare our computed results with the experimental data obtained for the Northrop F-5 platform by Tijdeman et al. at NLR.[22] Figures (5a)-(5c) present in-phase and out-of-phase pressures $\Delta C_p s$ at two span stations ($Y=0.181$ and 0.50) at low reduced frequencies ($K=0.1$ and 0.11). The present results compare fairly well with Tijdeman's data, particularly for the out-of-phase pressures. It is in-

Table 4 AGARD wing-tail interference $Z_{TAIL}=0.6$ at $M=3.0$ and $K=1.5$

Methods Elements		Present (100)	Present (50)	Ref. 6 (170)	Ref. 18
Q_{11}	MOD	0.2345	0.2427	0.2512	0.2375
	ARG	64.73	66.36	68.57	67.40
Q_{21}	MOD	0.3972	0.4281	0.4335	0.4029
	ARG	22.58	26.89	21.60	19.35
Q_{31}	MOD	0.1325	0.1361	0.2616	0.1504
	ARG	51.47	56.56	58.93	33.55
Q_{41}	MOD	0.1008	0.1042	0.1863	0.1180
	ARG	61.55	66.32	63.55	43.47
Q_{12}	MOD	0.0908	0.0982	0.0905	0.0872
	ARG	136.7	136.1	150.71	148.82
Q_{22}	MOD	0.3664	0.3842	0.4026	0.3742
	ARG	97.55	98.92	103.68	101.23
Q_{32}	MOD	0.1006	0.1063	0.2009	0.1045
	ARG	121.0	120.8	129.58	118.02
Q_{42}	MOD	0.0776	0.0820	0.1457	0.0833
	ARG	123.7	123.4	130.66	119.16
Q_{33}	MOD	0.3983	0.3965	0.3995	0.3936
	ARG	86.45	86.9	87.62	87.63
Q_{43}	MOD	0.2750	0.2751	0.2761	0.2797
	ARG	87.14	88.32	88.80	88.52
Q_{34}	MOD	0.5504	0.5638	0.5349	0.5253
	ARG	32.43	34.97	30.54	30.03
Q_{44}	MOD	0.4800	0.4829	0.4555	0.4531
	ARG	51.45	52.66	49.35	47.28

teresting to observe that the measured in-phase pressures appear to be "wavy." We believe that the waviness of ΔC_p is typical of nonlinear unsteady supersonic flow (e.g., see Fig. 19 of Ref. 10), which is beyond the prediction capability of the present linear theory.

V. Conclusion

It has been shown that the H-G method has the following advantages over the previous unsteady supersonic methods:

1) The formulation of H-G method is a consistent one; it is general in the frequency domain.

2) The H-G method procedure is versatile in handling planar and coplanar as well as nonplanar planforms.

3) The required number of panel elements is least affected of all the procedures by the given Mach number and reduced frequencies.

4) The required number of panel elements is only a fraction of those required by previous PGM methods.

For these reasons, we believe that a computationally efficient, cost-effective method for unsteady supersonic three-dimensional flow prediction is finally in hand. Once fully developed, the H-G method could very well complement the doublet-lattice method in subsonic flow. It would provide the aircraft industry with an effective tool for aeroelastic applications in supersonic flow.

Further research effort in developing the H-G method is still required. For example, in the general frequency domain, an effective method that can handle unsteady flow for bodies of revolution and for wing-body combinations is still lacking. Related research areas include the low-supersonic flow regime, where nonlinearity is important. Although from a practical standpoint this nonlinear flow regime is of primary importance, research efforts in the past have not been fruitful in offering an effective method accounting for the three-dimensional nonlinearity. Continuing effort to extend the H-G method toward this end is in progress.

Acknowledgments

The planar case of the present work was developed while both authors were employed at Northrop Aircraft Division; the nonplanar case was investigated at Arizona State University under the University Grant-in-Aid funding. The authors would like to acknowledge the support provided by both institutions.

The authors would like to thank Dr. William P. Rodden for helpful discussion and valuable suggestions. The first author (PCC) would like to thank Mr. Sheldon Schwartz of Northrop for encouragement and continuous support during the course of the research. In particular, PCC is indebted to Dr. Kari Appa of Northrop for his initiation of the problem during the preliminary phase of the present development.

References

[1]Rodden, W. P., Giesing, J. P., and Kalman, T. P., "New Developments and Applications of the Subsonic Doublet-Lattice Method for Nonplanar Configurations," AGARD Symposium on Unsteady Aerodynamics for Aeroelastic Analyses of Interfering Surfaces, Paper No. 4, May 1970.

[2]Giesing, J. P. and Kalman, T. P., "Oscillatory Supersonic Lifting Surface Theory Using a Finite Element Doublet Representation," AIAA Paper 75-761, 1975.

[3]Cunningham, A. M. Jr., "Oscillatory Supersonic Kernel Function Method for Interfering Surface," *Journal of Aircraft*, Vol. 11, No. 11, 1974, pp. 664-670.

[4]Cunningham, A. M. Jr., "Oscillatory Supersonic Kernel Function Method for Isolated Wings," *Journal of Aircraft*, Vol. 11, No. 10, 1974, pp. 609-615.

[5]Jones, W. P. and Appa, K., "Unsteady Supersonic Aerodynamic Theory for Interfering Surfaces by the Method of Potential Gradient," NASA CR-2898, 1977.

[6]Hounjet, M. H. L., "An Improved Potential Gradient Method to Calculate Airloads on Oscillating Supersonic Interfering Surfaces," *Journal of Aircraft*, Vol. 19, No. 15, 1982.

[7]Jones, W. P., "Supersonic Theory for Oscillating Wings of Any Planforms," British Aeronautical Research Council R&M 2655, June 1948.

[8]Harder, R. L. and Rodden, W. P., "Kernel Function for Non-Planar Oscillating Surfaces in Supersonic Flow," *Journal of Aircraft*, Vol. 8, No. 8, Aug. 1971, pp. 677-679.

[9]Desmarais, R. M., "An Accurate and Efficient Method for Evaluating the Kernel of the Integral Equation Relating Pressure to Normal Wash in Unsteady Potential Flow," AIAA Paper 82-0687, 1982.

[10]Liu, D. D. and Pi, W. S., "Transonic Kernel Function Method for Unsteady Flow Calculations Using a Unified Linear Pressure Panel Procedure," AIAA Paper 80-0737-CP, 1980.

[11]Chadwick, W. R., "Unsteady Supersonic Cascade Theory Including Nonlinear Thickness Effects," Ph.D. Thesis, Naval Postgraduate School, June 1975; see also AGARD CP-177, Sept. 1975.

[12]Jordan, P. F., "Aerodynamics Flutter Coefficients for Subsonic, Sonic and Supersonic Flow (Linear Two-Dimensional Theory)," Aeronautical Research Council R&M 2932, 1957.

[13]Laschka, B., "Der harmonisch Schwingende Rechteckflugel bei Uberschallstromung," Ernst Heinkel Flugzugbau, GmbH, Rept., 1960.

[14]Stark, V. J. E., "Calculation of Aerodynamic Forces on Two Oscillating Finite Wings at Low Supersonic Mach Numbers," SAAB Tech. Note TN 53, 1964.

[15]Fenain, M. and Guiraud-Vallee, D., "Numerical Calculations of Wings in Steady or Unsteady Supersonic Flow, Part 1: Steady Flow; Part 2: Unsteady Flow," *Recherche Aerospatiale,* No. 115, 1966-67.

[16]Woodcock, D. L., "Comparison of Methods Used in Lifting Surface Theory," AGARD Rept. 583, Jan. 1971.

[17]Tseng, K. and Morino, L. "A New Unified Approach for Analyzing Wing-Body-Tail Configuration with Control Surfaces," AIAA Paper 76-418, 1976.

[18]Pollock, S. J. and Huttsell, L. J., "Applications of Three Unsteady Aerodynamics Load Prediction Methods," AFFDL TR-73-147, May 1974.

[19]Mykytow, W. J., Olsen, J. J., and Pollock, S. J., "Application of AFFDL Unsteady Load Prediction Method to Interfering Surfaces," AGARD Symposium on Unsteady Aerodynamics for Aeroelastic Analyses of Interfering Surfaces, Tonsberg, Norway, AGARD Cp-80-71, Paper No. 7, 1970.

[20]Jones, R. T. and Cohen, D., *High Speed Wing Theory,* No. 6 Princeton Aeronautical Paperbacks, Princeton University Press, Princeton, N. J., 1960, pp. 156-157.

[21]Miles, John W., *The Potential Theory of Unsteady Supersonic Flow,* Cambridge University Press, Cambridge, Mass. 1959, pp. 128-149.

[22]Tijdeman et al., "Transonic Wind-Tunnel Tests on an Oscillating Wing with External Store," Part II: "The Clean Wing," NLR TR-78106U.

[23]Jordan, P. F., "Numerical Evaluation of the Three-Dimension Harmonic Kernel," *Zeitschrift für Flugwissenschaften* 24 Heft 4, 1976, pp. 205-209.